ACS Catalysis

pubs.acs.org/acscatalysis Research Article

Relationship between the Surface Reconstruction of Nickel Phosphides and Their Activity toward the Hydrogen Evolution Reaction

Sayan Banerjee, Arvin Kakekhani, Robert B. Wexler, and Andrew M. Rappe*

Cite This: *ACS Catal.* 2023, 13, 4611−4621 Read Online

ABSTRACT: Nickel phosphides (Ni_xP_y) are a class of materials that are made out of earth abundant elements and have shown relatively high hydrogen evolution reaction (HER) activity. Here, we perform first-principles density functional theory (DFT) calculations to systematically investigate the stoichiometric and nonstoichiometric surface reconstructions of six different Ni_xP_y, i.e., Ni_3P, $Ni_{12}P_5$, Ni_2P, Ni_5P_4, NiP_2, and NiP_3, under electrochemical conditions and to illustrate the implications of such reconstructions for the catalytic activity toward HER. Our results can explain a broad range of experimental observations on the HER activity of Ni_xP_y in a unified framework. For the majority of cases, our protocol can closely reproduce the experimentally measured overpotential trends in the literature, which validates its usefulness in generating physical insight into the surface phenomena responsible for HER activity. We find that, among the Ni_xP_y studied here, Ni_3P and Ni_5P_4 are the most active catalysts toward HER in acid, whereas Ni_5P_4 performs the best compared to other Ni_xP_y in base, in agreement with previous experimental reports. We show that P-vacancy formation in base renders the Ni-rich Ni_xP_y (Ni_3P, $Ni_{12}P_5$, Ni_2P, and Ni_5P_4) worse performers in base when compared to their activity in acid and hence propose that introducing nonmetals, which are less prone to dissolution, can improve their catalytic performance. In terms of active site design, we find Ni_3 hollow sites bind H too strongly and surface P sites with P−Ni bonds bind H too weakly. On the other hand, we identify that surface P sites with P−P bonds offer the best catalytic performances, and therefore, we predict that active site engineering to maximize the abundance of such surface motifs can further improve the HER activity. Moreover, we unravel the nature of H binding across the material class for different binding motifs via electronic structure theory analysis. The chemical insight we provide in this work can help rationalize the search for materials composed of inexpensive earth abundant elements that provide improved HER catalytic activity.

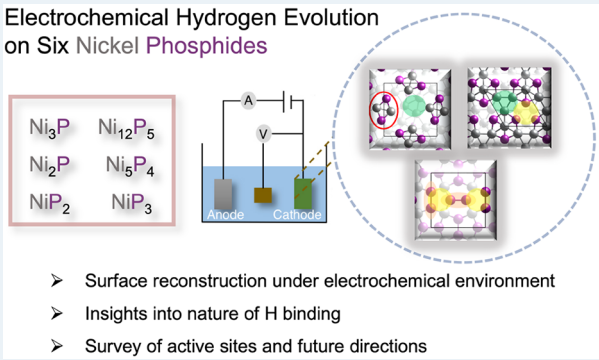

KEYWORDS: *hydrogen evolution reaction, surface reconstruction, electrocatalysis, nickel phosphides, earth-abundant maetrials*

■ INTRODUCTION

Designing stable and active hydrogen evolution catalysts using water as the proton source is a crucial ingredient of green and renewable energy technology.[1,2] Pt has been shown to be the most active hydrogen evolution reaction (HER) catalyst due to its ability to offer thermoneutral H binding on the surface and facile kinetics.[3−6] Pt also offers high stability under electrochemical conditions. However, the high cost of Pt is one of the main bottlenecks of using it as a viable and scalable HER catalyst. To this end, the development of HER catalysts made from earth-abundant elements is regarded as one of the sustainable alternatives.[3,7−21] Nickel phosphide (Ni_xP_y) catalysts have been developed as potential substitutes for Pt. Several Ni_xP_y, including Ni-rich ($x > y$) and P-rich ($x < y$) systems, have been synthesized and demonstrated to show reasonable activity and stability for HER.[3,13−21]

Surface reconstruction is a class of phenomena where solid surfaces undergo geometric, electronic, and atomic changes to minimize the surface free energy, e.g., by passivating under-coordinated surface atoms.[13,22−25,27−36] Atomic surface reconstruction can be stoichiometric, where the surface stoichiometry mirrors the bulk termination stoichiometry, and it can also be nonstoichiometric, where surfaces have different stoichiometry than the bulk. Several studies have shed light on how surface reconstructions can influence the catalytic activity of heterogeneous reactions.[13,22,26,30,33−35,37] For electrochemical reactions, reaction conditions such as pH and electrode potential (U) can change the surface structure

Received: January 17, 2023
Revised: March 4, 2023

   https://doi.org/10.1021/acscatal.2c06427
ACS Catal. 2023, 13, 4611−4621

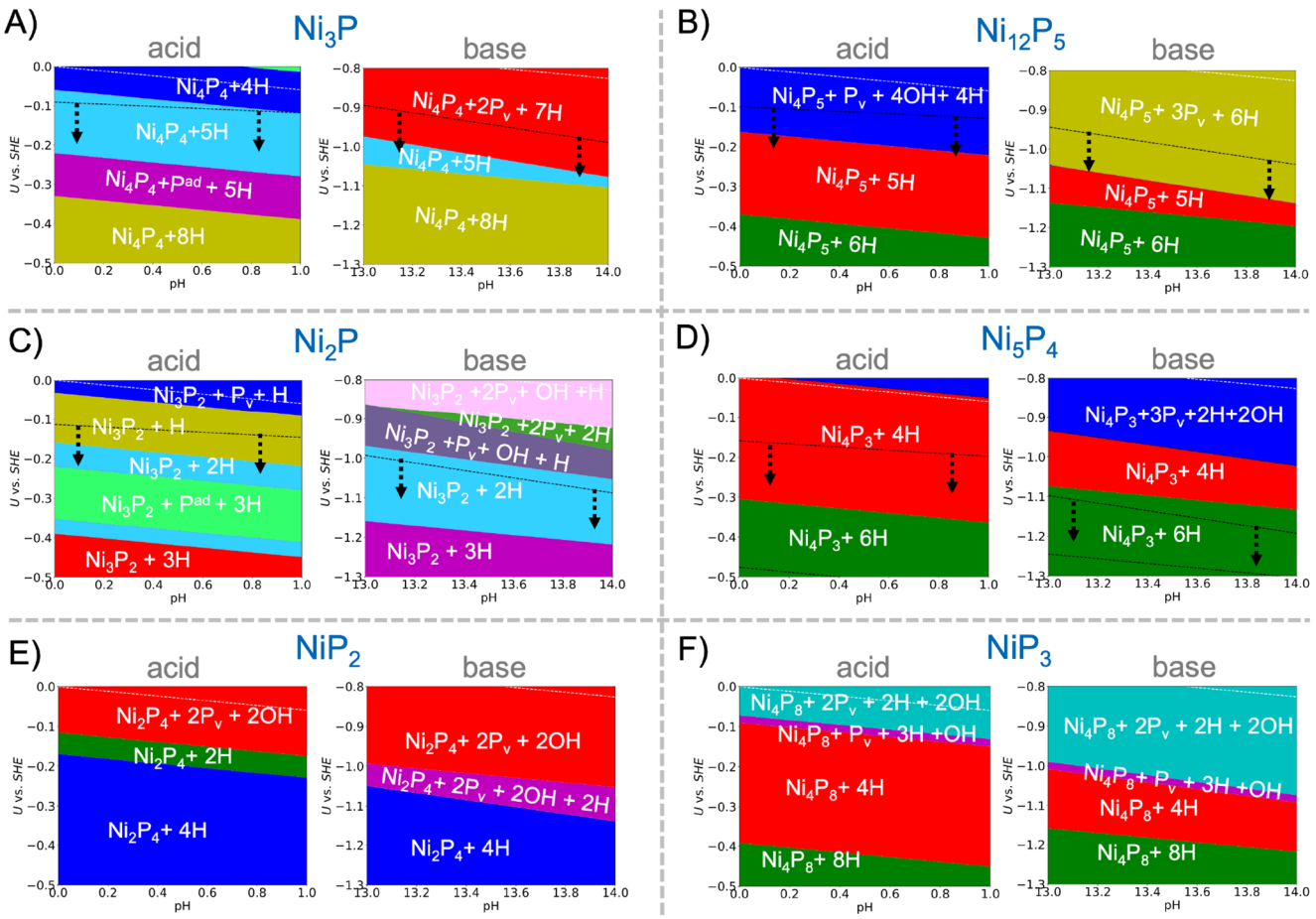

Figure 1. Surface phase diagram in acidic and basic conditions for (A) Ni_3P, (B) $Ni_{12}P_5$, (C) Ni_2P, (D) Ni_5P_4, (E) NiP_2, and (F) NiP_3. SHE stands for standard hydrogen electrode. The notation is (bulk: surface termination + adsorbates), for example, $Ni_{12}P_5$: Ni_4P_5+5H corresponds to the material $Ni_{12}P_5$ with the surface termination Ni_4P_5, and the surface is hydrogenated by 5H. P_v:, P vacancy; P_{ad}, P adatom. Dashed black line is the boundary of the bulk stability region (which lies on the side indicated by the black arrows), and white dashed line indicates 0 V vs reversible hydrogen electrode (RHE) line. The diagrams are constructed by studying the surface unit cell for each of the compositions.

and reconstruction dynamically.[30,38,39] In this regard, transition metal phosphides (TMPs) including Ni_xP_y have been shown to undergo various surface reconstructions under electrochemical conditions, and furthermore, such reconstructed surfaces are found to exhibit different catalytic properties than bulk-terminated surfaces.[13,30,40]

TMPs have garnered significant interest because of the availability of multiple binding motifs including metal (e.g., Ni) and nonmetal sites (P) combined with their metallic nature.[7,41−43] Additionally, the covalent bonding between the metal and nonmetal in a TMP can offer interesting chemistry, which is not present in pure transition metals or metallic alloys.[44,45] Experimentally, a class of Ni_xP_y catalysts including Ni_3P,[13] $Ni_{12}P_5$,[15,18,46] Ni_2P,[3,15,19,20] Ni_5P_4,[14] and NiP_2[47,48] have been shown to exhibit HER activity. Furthermore, computational studies have been conducted to understand the HER activity of Ni_xP_y,[13,30] although only a few studies explicitly consider the pH- and *U*-dependent surface reconstructions and the consequence of such reconstructions on catalytic performance. Only Ni_2P and Ni_5P_4 have been studied using such an approach;[30] there has not been any first-principles report on Ni_3P, $Ni_{12}P_5$, NiP_2, and NiP_3. Therefore, there is a need for a study that systematically explores the surface reconstruction of different Ni_xP_y as a class and relates that to their HER activity.

On the another hand, as Ni_xP_y offers a diverse set of binding motifs, understanding the H binding strength across the series is essential to design a more efficient Ni_xP_y-based HER catalyst.[13,30,44] The available binding motifs include Ni_3 hollow sites, P_3 hollow sites, Ni top, P top, and bridging sites between Ni−Ni, Ni−P, and P−P. Such diversity introduces additional complexity in comparison to metal-based systems. Furthermore, as different orbitals participate in the hybridization with the adsorbed H at the various metal and nonmetal sites, traditional descriptors such as the d-band model cannot provide physically meaningful insights.[49−52] Therefore, an electronic structure theory analysis to understand the nature of H binding at different active sites is required to rationally design improved TMPs for HER.

In this work, we study the surface reconstruction and HER activity of six different Ni_xP_y, i.e., Ni_3P, $Ni_{12}P_5$, Ni_2P, Ni_5P_4, NiP_2, and NiP_3, wherein the materials considered represent both Ni- and P-rich ends of the compositional space. We investigate the pH- and *U*-dependent surface reconstruction and decipher their effect on the HER activity using first-principles density functional theory (DFT) calculations. The results successfully reproduce a set of experimental observations of Ni_xP_y HER catalysts spanning the last two decades. Moreover, we present a survey on HER activity and nature of the active sites to provide future directions on what sites

https://doi.org/10.1021/acscatal.2c06427
ACS Catal. 2023, 13, 4611−4621

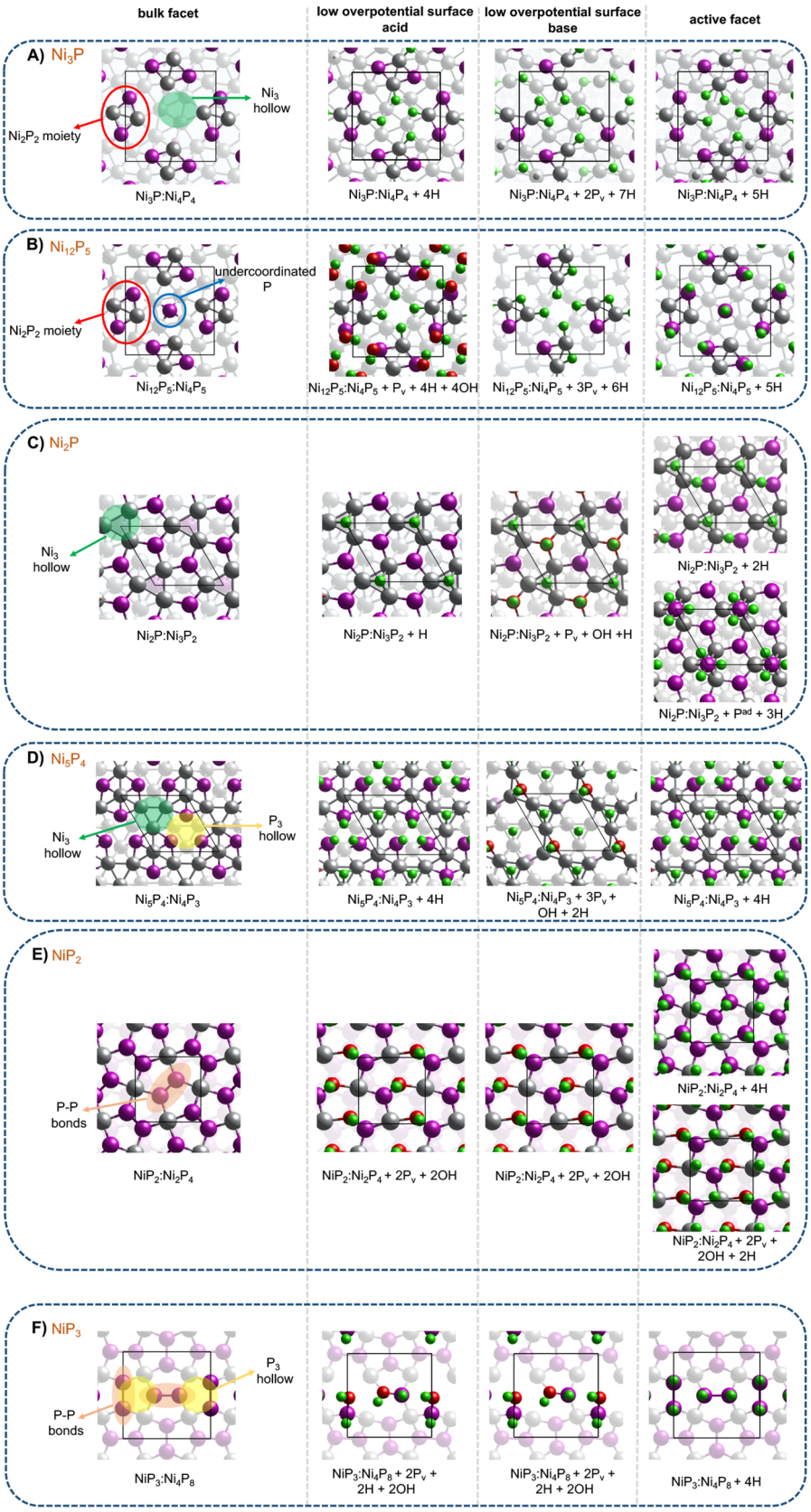

Figure 2. Column 1 shows the bulk-like low energy surface terminations of the Ni_xP_y, column 2 shows the DFT predicted surface termination post reconstruction at zero overpotential in acid and column 3 in base. Column 4 shows the HER active surface(s).

https://doi.org/10.1021/acscatal.2c06427
ACS Catal. 2023, 13, 4611−4621

should be maximized in Ni_xP_y to further improve their performance. Finally, we perform electronic structure density of states (DOS) analyses to understand the H binding energy across the studied Ni_xP_y materials set and different binding motifs. We hope that our results and the generated physical and chemical insights in this work can provide a pathway to engineer the surface structure and active sites to further improve the design of earth-abundant HER catalysts.

■ RESULTS AND DISCUSSIONS

Surface Phase Pourbaix Diagrams of Ni_xP_y. Previous experimental and theoretical studies have shown that (001)/(0001)/(000$\bar{1}$) facets are stable and catalytically active factes for Ni_3P, Ni_2P, and Ni_5P_4; thus here we perform DFT calculations on these low Miller index facets.[3,13,30,53−56] While we acknowledge that other facets could also play a role for $Ni_{12}P_5$, NiP_2, and NiP_3, we focus on such low-index facets as a tractable set of calculations to study all six Ni_xP_y. Additionally, the widely used high-temperature solid-state synthesis of Ni_xP_y allows the structure to fully equilibrate, thereby exposing the thermodynamically preferred facets predominantly and avoiding kinetically controlled high-energy facets.[13,14] Such energetically preferred facets have been reported to be mostly lower Miller index facets.[13] Next, we find out the stable surface terminations of the facets by calculating the surface energy of different terminations (see the Suppoting Information (SI) for more details).[53] We have found that the P-rich surface terminations are the most energetically favorable surface terminations of Ni_xP_y, which have also been reported previously.[30,53] Specifically here, we have studied the surface reconstruction and hydrogen evolution reaction (HER) activity of $Ni_3P(001):Ni_4P_4$, $Ni_{12}P_5(001):Ni_4P_5$, Ni_2P-$(0001):Ni_2P_3$, $Ni_5P_4(000\bar{1}):Ni_4P_3$, $NiP_2(001):Ni_2P_4$, and $NiP_3(001):Ni_4P_8$, where the notation is bulk-(facet):termination. A detailed discussion regarding the considered facets and surface terminations is provided in the Supporting Information. After establishing the stable termination, we construct the surface phase Pourbaix diagram by considering the aqueous equilibrium of Ni and P at different pH and electrode potentials (U) and by considering the H/O/OH adsorption on the surface. The theoretical details of establishing the surface phase Pourbaix digram is given in the Methods section. Thereafter, the energetics of the HER is studied on the most stable surface under the relevant electrochemical conditions. The theoretical overpotential/limiting potential (η) is calculated by finding out the minimum electrode potential required to render both HER steps (H adsorption on surface and H_2 formation) thermoneutral.[57] Note that we study the HER activity of different adsorbed surface H species, and the role of H of surface hydroxyl (−OH) species is not considered herein. Additionally, we have not considered the solvation effect and the role of pH and electrode potential in affecting the kinetics of HER.[58,59] Rather an *ab initio* thermodynamic perspective is presented to understand the HER activity by establishing the stable surface structures under relevant electrochemical conditions and quantifying their activity.

The surface-phase Pourbaix diagrams are given in Figure 1 for acidic and basic conditions for all the six Ni_xP_y. The considered surfaces span both stoichiometric and non-stoichiometric Ni_xP_y surfaces with H/OH/O adsorbates and a variety of coverages. The list of considered surfaces is given in the Supporting Information. As previous studies have shown that the nonmetal P plays a critical role in determining the HER catalytic activity,[13,30] we have extensively considered P-vacancy (P_v) and P-adatom (P_{ad}) formation in the surface structure database. The stable bulk termination, stable surfaces at low overpotential (η) in both acid and base, and the catalytically active surfaces, are shown in Figure 2.

Nature of Active Sites and Structure−Activity Relationship. *Surface Structure and Binding Motifs.* The simplest type of surface one can investigate is the bulk-like terminations of the material, in which one simply terminates the bulk-order of the material along the surface normal (here, defined by the Miller indices) and makes a surface. Although we know from the literature that such a naive approach neglects the (nonstoichiometric) atomic surface reconstruction phenomena, which are important in determining its catalytic activity, we begin our systematic study with the bulk-like surfaces. We later augment this knowledge to include the relevant atomic surface reconstructions. The bulk-like terminations of Ni_xP_y exhibit a rich set of active sites, which are shown in the leftmost column of Figure 2. In the Ni-rich Ni_xP_y, i.e., Ni_3P, $Ni_{12}P_5$, Ni_2P, and Ni_5P_4, Ni_3 hollow sites are ubiquitous on surface and subsurface. Such sites are shown as green shaded regions in Figure 2 in panels A, B, and C, and for $Ni_{12}P_5$, such sites are present at the subsurface. Along with the Ni_3 hollow sites, Ni_2P_2 moieties are present both in Ni_3P and $Ni_{12}P_5$ (red circles in the leftmost column in Figure 2). As the Ni_xP_y becomes more P-rich, the P_3 hollow sites (yellow shaded regions in Figure 2) and surface P−P bonds (light red shaded regions in Figure 2) begin to appear. For Ni_5P_4, which lies near the borderline of Ni-rich and P-rich, we find both Ni_3 and P_3 hollow sites (Figure 2D). Next, for P-rich Ni_xP_y, i.e., NiP_2 and NiP_3, P−P bonds are the most prominent motif (Figure 2E,F). The P-sites of NiP_2 and NiP_3 have broken tetrahedral coordination and are undercoordinated relative to the P of the P_3 hollow sites of Ni_5P_4.

We find that the presence of different binding sites on bulk-terminated surfaces results in a wide range of coordination environments for the adsorbed H; depending on the coordination environment, the H binding energy (ΔG_H) varies significantly. At the Ni_3 hollow sites, H acquires a 3-fold coordination (μ_3-H). On the other hand, P atoms of the P_3 hollow site and the P−P moiety offer μ_1-H top-site bonding. We find that, irrespective of the composition, Ni_3 hollow sites have strong H binding energy ($\Delta G_H \approx -0.45$ eV). On the other hand, P-sites offer a range of ΔG_H. Specifically, P-sites of surface P−P bonds (in NiP_2 and NiP_3) offer relatively stronger H binding ($\Delta G_H \approx -0.1$ to -0.3 eV) than the P-sites of Ni_2P_2 moieties ($\Delta G_H \geq 0$ eV). Further, P sites of the P_3 hollow can have near thermoneutral ΔG_H, along the findings of previous work.[30]

Catalytically Active Surfaces under Reaction Conditions. Although understanding the surface structure of the bulk-like terminations provides valuable insights, such structures can change dynamically under the electrochemical conditions.[30,38,39] As mentioned earlier, we include such effects by constructing the surface phase Pourbaix diagram. Here, we focus specifically on pH = 0 and pH = 14 to represent the acidic and basic conditions and to understand the pH effect on the surface structure from a thermodynamic perspective. By establishing the surface phase Pourbaix diagram (Figure 1), we determine the most active surface toward the HER at both the acidic and basic conditions. As a demonstrative example, for $Ni_{12}P_5$ in acidic condition (pH = 0) (Figure 1B), we find from

https://doi.org/10.1021/acscatal.2c06427
ACS Catal. 2023, 13, 4611−4621

the Pourbaix diagram that at a lower overpotential (near 0 V vs SHE) $Ni_{12}P_5$:Ni_4P_5+P_v+4OH+4H is the most stable surface (Figures 1B and 2B). As the hydrogen atoms are adsorbed at the Ni_3 hollow sites, they are not active toward HER at such condition because of strong binding energy ($\Delta G_H \approx -0.45$ eV). Here by "not active", we indicate that, in the potential window where this particular surface is stable, one cannot achieve both thermoneutral H adsorption and H_2 evolution.[30] Then, as the conditions become more reducing (more negative U), we see the emergence of $Ni_{12}P_5$:Ni_4P_5+5H as the stable surface (Figures 1B and 2B) and these H atoms are active toward HER with near thermoneutral H binding. Thus, for $Ni_{12}P_5$ in acid, we determine $Ni_{12}P_5$:Ni_4P_5+5H to be the active surface. In similar fashion, we first find out the HER active surfaces under acidic and basic conditions, by constructing the surface phase diagram. Thereafter, we calculate the thermodynamic overpotential (η) of the catalytically relevant surfaces near 0 V vs RHE, which are summarized in Figure 3. We find

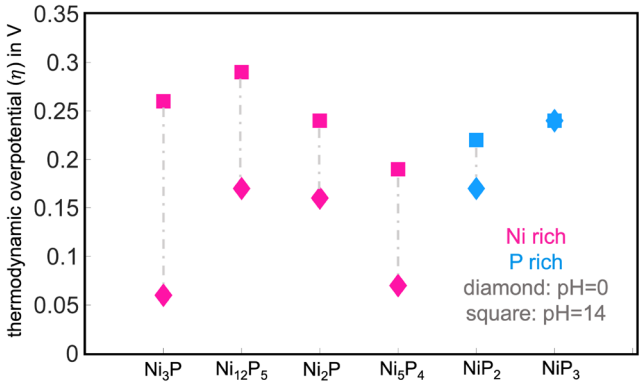

Figure 3. Summary of thermodynamic overpotentials (η) in acid and base. The η of Ni-rich and P-rich Ni_xP_y are shown using pink and blue markers, respectively. Diamond markers correspond to pH = 0 and square markers correspond to pH = 14.

that there exists broadly two different origins of the η. First, we find that, for some cases, the formation of the catalytically active surface determines the η. For example, the formation of $Ni_{12}P_5$:Ni_4P_5+5H or the formation of Ni_3P:Ni_4P_4+5H (Figures 1A and 2A) is rate limiting and can be ascribed as the origin of the η. In other words, the active surfaces appear only after a certain U, i.e., under more reducing conditions where the H can provide thermoneutral HER. On the other hand, for some situations, we find that the H atoms are strongly bound, and overpotential must be applied to attain thermoneutral binding.[30,57] Such a situation can be observed for Ni_2P:Ni_3P_2+H (Figures 1C and 2C) or for NiP_2:Ni_2P_4+2H (Figures 1E and 2E). Overall, we find that the pH and U have significant effects on the nature of the HER active surfaces. Additionally, we find that the nonstoichiometric surface reconstructions via P vacancy (P_v) and adatom (P_{ad}) formation at low overpotentials is a prevalent phenomenon for Ni_xP_y. The basic environment favors the formation of solvated phosphate species, thus increasing the thermodynamic tendency of the surfaces to host P vacancies. On the other hand, P-adatom surface reconstructions can happen in acidic media for Ni_2P and Ni_3P near the experimental conditions. Furthermore, at higher overpotentials, the stoichiometric surfaces with a range of H coverages are found to be the most common surfaces.

Trends in the HER Activity. By combining the information from surface phase diagrams and stable surfaces near the experimentally relevant conditions in acid and base, we calculate the overpotential (η) for six different Ni_xP_y under two different conditions, pH = 0 and pH = 14 (Figure 3). Therefore, we calculate a total of 12 η values, which are summarized in Figure 3. Here, we discuss the key trends observed in Figure 3. We compare the theoretically calculated values with a range of experimental measurements from the literature. Although we acknowledge that experimentally measured overpotentials can vary in different experiments, here, we focus on the key qualitative and quantitative trends that have been observed experimentally and then validate our theoretical results against them.

a. We find that, among the Ni-rich Ni_xP_y in acid, the HER activity trend is $Ni_3P \approx Ni_5P_4 > Ni_2P > Ni_{12}P_5$, where $Ni_{12}P_5$ has the highest η (Figure 3). Such a trend has also been observed experimentally in a set of previous reports (Table 1). Pan et al. reported the HER activity trend as $Ni_5P_4 > Ni_2P > Ni_{12}P_5$ (Table 1).[15] Accordingly, by combining the experimental observations by Popczun et al. on Ni_2P[3] and by Laursen et al. on Ni_5P_4[14] and Ni_3P,[13] the experimental trend of acidic HER is found to be the same (Table 1), i.e., $Ni_3P \approx Ni_5P_4 > Ni_2P > Ni_{12}P_5$. Therefore, our results successfully reproduce the experimental trends for Ni-rich Ni_xP_y for acidic HER (Table 1 and Figure 3). This supports our atomistic approach of understanding surface reconstruction using surface phase Pourbaix diagrams and binding sites for calculating the HER overpotentials.

Table 1. Comparing the Experimental η Required to Attain 10 mA/cm^2 of Current Density (obtained from the literature) and Predicted Theoretical Thermodynamic η in This Study

material	medium	η_{theory} (V)	η_{exp} (V)
Ni_3P	acid	0.06	0.07[13]
Ni_3P	base	0.26	0.29[13]
$Ni_{12}P_5$	acid	0.17	0.21[15]
$Ni_{12}P_5$	base	0.29	0.26[46]
Ni_2P	acid	0.16	0.14,[15] 0.13[62]
Ni_2P	base	0.24	0.24,[61] 0.18[63]
Ni_5P_4	acid	0.07	0.04,[14] 0.12[15]
Ni_5P_4	base	0.19	0.19[13]
NiP_2	acid	0.17	0.27,[48] 0.08[47]
NiP_2	base	0.22	0.25,[48] 0.10[47]
NiP_3	acid	0.24	NA
NiP_3	base	0.24	NA

b. Next, we observe highly pH-dependent changes in η for Ni-rich Ni_xP_y and almost pH-independent η for P-rich Ni_xP_y (Figure 3). This has also been observed in previous experimental reports (Table 1), where Ni-rich Ni_xP_y performs less well for alkaline HER than acidic HER[13,14,46,60,61] and P-rich Ni_xP_y performs equally in acid and base.[47,48] Hence, the results capture the pH-dependent η for different Ni_xP_y.

To gain more insight into the theoretically predicted η values and to understand the trends in Table 1 and Figure 3, we focus on their chemical origins and discuss the key insights below.

https://doi.org/10.1021/acscatal.2c06427
ACS Catal. 2023, 13, 4611−4621

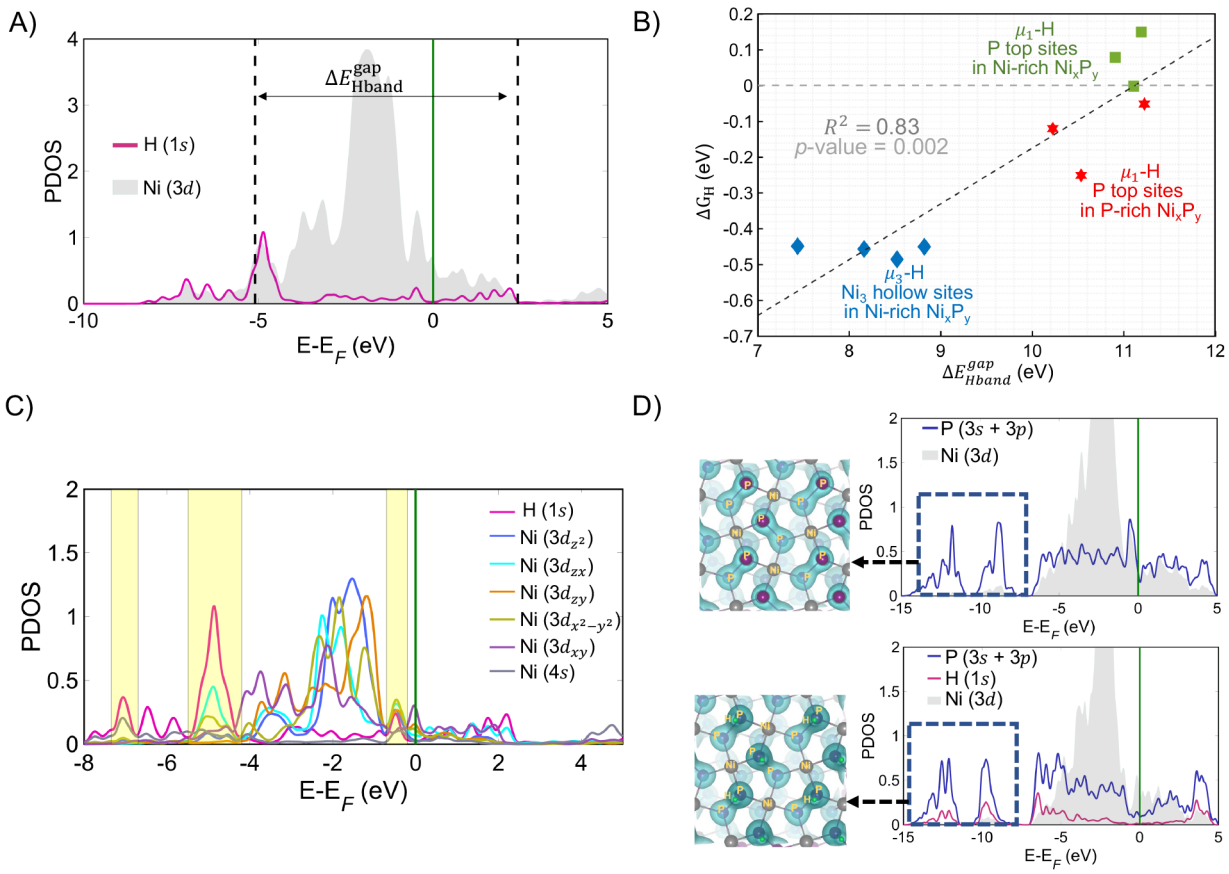

Figure 4. Insights into site-dependent H binding energy. (A) Schematic showing the definition of the ΔE^{gap}_{Hband}; eq 1 shows the explicit definition. (B) Correlation between ΔE^{gap}_{Hband} and ΔG_H, both calculated by DFT. Three different clusters corresponding to different H binding sites are shown. (C) Orbital resolution analysis between Ni 3d and 4s orbitals with H 1s at the Ni_3 hollow site of Ni_2P. The yellow shaded regions correspond to the places where more than one orbital of Ni hybridizes with H. (D) Existence of P−P bonds in P-rich Ni_xP_y provide states for H hybridization. The figure shows such phenomenon for NiP_2 as a demonstrative example. The projected density of states plots (PDOS) show the H hybridization with the P states, and integrated local density of states (ILDOS) analyses confirm that those states correspond to P−P hybridized states.

a. Ni_3P and Ni_5P_4 are the most active HER catalysts in acid (Figure 3), while Ni_5P_4 also has the lowest η in base (Figure 3). By contrast, for Ni_3P, η increases from 0.06 to 0.26 V between pH = 0 and pH = 14 (Figure 3). We find that, for the Ni_5P_4:Ni_4P_3 surface, there exists one Ni_3 hollow site and one P_3 hollow site per cell (Figure 2D). The first H* binds strongly at the Ni_3 hollow site, and the subsequent three hydrogenations happen at the P_3 hollow site. H* at the P_3 hollow site is found to be HER active for the Ni_5P_4:Ni_4P_3+4H surface. On the other hand, due to the relatively high concentration of Ni in Ni_3P, Ni_3 hollow sites are abundant, which results in strong H adsorption at low η in acid. We find that, due to the coverage effect, the Ni_3P:Ni_4P_4+5H becomes HER active. However, in base, P_v are formed, opening up more Ni_3 hollow sites in Ni_3P than Ni_5P_4, resulting in strong H* adsorption even at a higher coverage and the stabilization of the highly hydrogenated surface Ni_5P_4:Ni_4P_3+2P_v+7H at low η. This is comprehensible as P_v formation makes Ni at the hollow sites under-coordinated. This results in an increased η for Ni_3P in base. Even though Ni_3 hollow sites are also present in Ni_5P_4, the relatively smaller concentration of such sites leads to a less significant increase of η between acidic and basic conditions than that for Ni_3P (Figure 3).

b. We find that $Ni_{12}P_5$ is the worst performer among the Ni-rich Ni_xP_y in acid (Figure 3). Such a low catalytic performance has also been seen experimentally (Table 1). We find that, in acidic environments, the under-coordinated P of $Ni_{12}P_5$:Ni_4P_5 (Figure 2B) dissolves, leaving a P vacancy (P_v) and exposing the Ni_3 hollow site, which has strong H* binding. As this rather inert surface with P_v ($Ni_{12}P_5$:Ni_4P_5 + P_v + 4OH + 4H) is stable for a relatively higher potential window in acid (Figure 1A middle panel), $Ni_{12}P_5$ becomes the worst performer in acid among the Ni-rich Ni_xP_y (Figure 4).

c. We find that P vacancy (P_v) formation as one of the root causes for lowered catalytic activity of Ni-rich Ni_xP_y (Ni_3P, Ni_5P_4, Ni_2P, and $Ni_{12}P_5$) in the basic medium[13,14,46,60,61] as the P_v formation results in more available Ni_3 hollow sites on the surface, which bind H too strongly. For example, the P_v formation in Ni_5P_4:Ni_4P_3 results in the removal of HER active P_3 hollow sites and exposes the subsurface Ni_3 hollow sites (Figure 2D, panel 3). Hence, we propose that introducing nonmetals that are less prone to dissolution can improve the HER activity in base for Ni-rich Ni_xP_y. For the P-rich Ni_xP_y (NiP_2 and NiP_3), surface P vacancies can form in both acidic and basic environments. Nevertheless, the lack of Ni_3 hollow sites (a consequence of Ni-poor composition) and the presence

https://doi.org/10.1021/acscatal.2c06427
ACS Catal. 2023, 13, 4611−4621

of some HER-active surface P species (forming P−P bonds) on NiP_2 and NiP_3 lead to an almost pH-independent HER activity (Figure 3), which has also been observed experimentally.[47,48]

d. We find that the effectively repulsive H−H (coverage-dependent) interactions can help create near-thermoneutral H binding sites once the H coverage per surface unit cell (s.u.c.) is relatively large, which is in accordance with previous works.[30] Such a situation is encountered for Ni_3P and Ni_5P_4 in acidic conditions, where the H binding energy (ΔG_H) at low coverage is exergonic (strong binding side of Sabatier volcano), but by going to slightly more reducing conditions and more H adsorption, the ΔG_H is rendered thermoneutral. For example, (Ni_3P:Ni_4P_4 + 4H) cannot provide thermoneutral H at lower overpotential, whereas (Ni_3P:Ni_4P_4 + 5H) has thermoneutral H near its stability region (Figures 1 and 2A). One should note that the magnitude of this effect is only large enough to push slightly overbound species toward thermoneutral binding. In basic conditions, P-vacancy formation creates such strong H-binding that it cannot become thermoneutral merely by coverage effects for Ni-rich Ni_xP_y at lower overpotential in basic conditions.

Insights into the Nature of H Binding and Active Sites. *Understanding the Electronic Driving Force for H Binding.* In the previous sections, we have shown that the H binding energy varies significantly depending on the nature of the active sites. Here, we provide an electronic structure theory-based analysis to understand the site-dependence of H binding. Specifically, we seek to understand how the binding motifs offer different electronic environments for H binding, for example, why Ni_3 hollow sites bind H strongly irrespective of the Ni_xP_y material or why P sites of Ni-rich and P-rich Ni_xP_y have different H binding energies. We find that the gap (ΔE^{gap}_{Hband}) between the center of the H band above and below of the Fermi energy (E_F), calculated using projected density of states calculations, is correlated with the H binding energy (ΔG_H) (Figure 4) with the R^2 = 0.83 and p-value = 0.002. In other words, ΔE^{gap}_{Hband} is the gap between the center of the filled H states and the center of the empty H states.

$$\Delta E^{gap}_{Hband} = \frac{\int_{E_F}^{\infty} \rho_{1s}(E)E\mathrm{d}E}{\int_{E_F}^{\infty} \rho_{1s}(E)\mathrm{d}E} - \frac{\int_{-\infty}^{E_F} \rho_{1s}(E)E\mathrm{d}E}{\int_{-\infty}^{E_F} \rho_{1s}(E)\mathrm{d}E} \quad (1)$$

A larger ΔE^{gap}_{Hband} corresponds to a more directional covalent bond formation, as it involves more orbital overlap, which results in separated bonding and antibonding regions. H binding at the Ni_3 hollow sites has the lowest ΔE^{gap}_{Hband} (Figure 4), which suggests that the bonding at Ni_3 hollow sites does not involve considerable orbital hybridization. Such a trend is robust for the Ni-rich Ni_xP_y where Ni_3 hollow sites are present, i.e., Ni_3P, $Ni_{12}P_5$, Ni_2P, and Ni_5P_4. In terms of orbital hybridization, 1s of H interacts with all the Ni 3d and 4s orbitals and therefore results in a delocalized nondirectional interaction. This is confirmed from the orbital projected DOS analysis, and the major overlap regions are shown in yellow shading in Figure 4C. The adsorbed H* at Ni_3 hollow sites is hydridic in nature (see Table S1 in the Supporting Information), which is in accordance with the previous results.[30,39] Therefore, due to the hydridic nature of the bound H* at electropositive Ni_3 hollow sites, it experiences electrostatic stabilization in a μ_3-coordinated geometry. Such a delocalized nondirectional interaction along with electrostatic favorability result in a strong H* binding (Figure 4B).

On the other hand, H binding at the P sites is associated with a larger ΔE^{gap}_{Hband} (Figure 4B) and therefore involves more orbital overlap, which results in separated bonding and antibonding regions. Furthermore, a higher ΔE^{gap}_{Hband} suggests a greater hybridization and perturbation of the surface electronic structure. For H binding at the surface P atoms for P-rich Ni_xP_y (NiP_2 and NiP_3) and at the P_3 hollow site of Ni_5P_4, the existence of relatively unstable surface P−P bonds renders the formation of H−P−P moieties thermodynamically favorable (Figure 4B,D). The stabilization originates from the stabilization of the antibonding states way below the Fermi energy, and such states correspond to the P−P bonds, as confirmed via the PDOS and integrated local density of states analysis (Figure 4D). On another hand, the P−H binding resulting in a H−P−Ni moiety in the absence of the surface P−P bonds (for Ni_3P, $Ni_{12}P_5$, Ni_2P) is a thermodynamically unfavorable phenomenon ($\Delta G_H > 0$) due to the lack of the relatively unstable P−P bonds in such situations. Additionally, we find that H adsorbed at the P sites (both with H−P−P and H−P−Ni moieties) has near zero charge (see Table S1 in the Supporting Information). Therefore, the extent of ionic bonding for surface P−H bonds is less than that of the surface Ni−H bonds at Ni_3 hollow sites where H is hydridic in nature. Hence, we find that the ΔE^{gap}_{Hband} serves as a strong descriptor for understanding H binding because it captures the vital aspects of H bonding, including the differences in covalency as well as ionicity, as revealed by H Löwdin charge calculations. Interestingly, similar interplay of covalent and electrostatic interactions has also been found for H binding at transition metal single-atom catalysts.[64] In summary, we observe that, for Ni_3 sites, H binding involves a higher extent of electrostatic stabilization and delocalized covalent binding at a μ_3-coordinated geometry; on the other hand, P sites offer strong hybridization with H 1s at a μ_1-coordinated geometry and lesser extent of ionic interaction.

Future Directions for Active Site Engineering. We observe that the H bonding on the Ni_xP_y metallic surfaces prefers a more delocalized metallic interaction rather than a more covalent one. Although, when such delocalized H binding can happen, i.e., at the Ni_3 hollow sites, H binding is found to be too strong and thereby not optimal. On the other hand, H binding at the P sites with H−P−Ni bonds is too weak and requires higher overpotential to become hydrogenated. Finally, we generally observe that, between the two limits of (too) strong H−Ni_3-hollow and (too) weak H−P−Ni bonds, P sites, which form surface P−P bonds, can be the optimal active sites for performing HER. Specifically, P_3 hollow sites offer near thermoneutral H binding, as a consequence of both surface P−P bonds and also as three P atoms are present, coverage effect plays a crucial role in making the third H to be adsorbed weakly. Hence, we propose that, to go beyond Ni_5P_4 for HER (which is the best Ni_xP_y so far reported), surface site engineering to maximally expose P_3 hollow sites for catalysis can be explored. Such active site engineering can help narrow the performance gap between Ni_xP_y and Pt.

■ CONCLUSIONS

Overall, we observe that, by exploring the compositional phase space of Ni_xP_y via varying the Ni/P ratio, the HER activity can be altered significantly. We present an atomistic computational

https://doi.org/10.1021/acscatal.2c06427
ACS Catal. 2023, 13, 4611−4621

protocol to predict the electrochemical activity of such surfaces toward HER activity, leading to the close correspondence between the overpotentials and trends predicted by such approach and the experimental results reported in the literature. We illustrate that, under varying electrochemical environments, the stoichiometry of the surfaces changes as a function of pH and electrode potential, and this stoichiometry change also significantly affects the reactivity in comparison to the bulk-like terminations. Additionally, we show that, as a result of multiple binding motifs on the surfaces, H coverage plays a critical role in determining the HER activity of Ni_xP_y. It is found that the Ni-rich Ni_xP_y exhibit pH-dependent thermodynamic overpotentials, while P-rich Ni_xP_y show almost pH-independent activity. We reveal that such dependence originates because of the nonstoichiometric surface reconstruction via P-vacancy formation, and we propose that introducing nonmetals that are less prone to dissolution can improve the alkaline HER activity. The nonmetal sites are found to be crucial and more active toward HER and therefore provide an additional dimension to design better HER catalysts beyond the monometallic compounds and metallic alloys. Moreover, we propose that the abundance of surface P_3 hollow sites can be further engineered to improve the HER activity and help narrow the gap between Ni_5P_4 and Pt. The unified framework demonstrated in this work to understand the HER on transition metal phosphides can guide the future design of improved and scalable earth-abundant HER catalysts.

METHODS

Density Functional Theory (DFT) Calculation Details. All of the density functional theory (DFT) calculations were performed using the Quantum ESPRESSO software package.[65] The generalized gradient approximation of Perdew, Burke, and Ernzerhof (PBE) was used to calculate the electronic exchange-correlation energy.[30,66−68] We chose a kinetic energy cutoff of 50 Ry to achieve necessary convergence for the calculated binding energies. The OPIUM (version 3.7) software was used to generate designed, optimized, norm-conserving, nonlocal pseudopotentials.[69−71] The DFT-D3 correction developed by Grimme et al. was used to capture dispersion interactions, which are important to the energetics of catalytic transformations.[72−76] Material-specific details are provided in the Supporting Information. We used the computational hydrogen electrode model to calculate the pH and potential dependence of the free energies of the reaction intermediates.[77,78]

Construction of the Surface Phase Diagrams. We construct the surface phase diagrams (Figure 1) by considering that each surface atom type A is in equilibrium with the aqueous solution and by implementing the computational hydrogen electrode model. This approach is adapted from the literature and has been demonstrated to be able to capture the pH- and U-dependent surface reconstructions.[30,38,79] For such event, the chemical equation is

$$S - A + n_w H_2O \rightleftharpoons S + [H_xAO_y]^z + n_H H^+ + n_e e^- \quad (2)$$

S is the surface (of the Ni_xP_y), n_w is the number of water molecules involved in the dissolution of A, $[H_xAO_y]^z$ is most stable (minimum Gibbs energy) form of A in the aqueous phase and z is its net charge, and n_H and n_e are the numbers of protons and electrons, respectively, produced in the dissolution of A.

The free energy change for the reaction 2:

$$\Delta G_{(A,diss)} = (G_S - G_{SA}) + (G_{[H_xAO_y]^z} + n_H G_H + n_e G_e - n_w G_{H_2O}) \quad (3)$$

Now expressing the dissolution eq 3 in terms of the standard state of A:

$$\Delta G_{(A,diss)} = (G_S + G_{A(std)} - G_{SA}) + (G_{[H_xAO_y]^z}) + n_H G_H + n_e G_e - n_w G_{H_2O} - G_{A(std)}) \quad (4)$$

Equation 4 can be expressed as desorption energy ΔG_{dsrp} for A and as $\Delta G_{A(std)/[H_xAO_y]^z}$ where A is in equilibrium with $[H_xAO_y]^z$:

$$\Delta G_{A,diss} = \Delta G_{dsrp} + \Delta G_{A(std)/[H_xAO_y]^z} + k_B T \ln a_{[H_xAO_y]^z} - 2.303 n_H k_B T \times pH - n_e q_e U \quad (5)$$

Next, we generate the surface phase Pourbaix diagrams using the expression in eq 5 where ΔG_{dsrp} is calculated using density functional theory. The bulk stability region (shown using black dotted lines and arrows in Figure 1) is calculated by considering the free energy change for the complete dissolution of the bulk Ni_xP_y phase,

$$\Delta G_{(Ni_xP_y,diss)} = -\Delta G^f_{Ni_xP_y} + x\Delta G_{Ni(s)/[H_xAO_y]^z} + y\Delta G_{P(s,white)/[H_xPO_y]^z} \quad (6)$$

where $\Delta G^f_{Ni_xP_y}$ is the free energy of formation of Ni_xP_y. The criterion for bulk stability is $\Delta G_{Ni_xP_y,diss} > 0$, and the bulk stability boundary is defined as (black dotted lines and arrows in Figure 1)

$$\Delta G^f_{Ni_xP_y} \leq x\Delta G_{Ni(s)/[H_xAO_y]^z} + y\Delta G_{P(s,white)/[H_xPO_y]^z} \quad (7)$$

ASSOCIATED CONTENT

Supporting Information

The Supporting Information is available free of charge at https://pubs.acs.org/doi/10.1021/acscatal.2c06427.

Discussions of computational details, surface energy calculation, and additional theoretical details, figures of side and top views of structures and surface structures, and table of Löwdin charge of H* at various binding sites on Ni_xP_y (PDF)

AUTHOR INFORMATION

Corresponding Author

Andrew M. Rappe − *Department of Chemistry, University of Pennsylvania, Philadelphia, Pennsylvania 19104-6323, United States;* orcid.org/0000-0003-4620-6496; Email: rappe@sas.upenn.edu

Authors

Sayan Banerjee − *Department of Chemistry, University of Pennsylvania, Philadelphia, Pennsylvania 19104-6323, United States;* orcid.org/0000-0002-8586-9236

Arvin Kakekhani − *Department of Chemistry, University of Pennsylvania, Philadelphia, Pennsylvania 19104-6323, United States;* orcid.org/0000-0002-8553-7776

https://doi.org/10.1021/acscatal.2c06427
ACS Catal. 2023, 13, 4611−4621

Robert B. Wexler − *Department of Chemistry, University of Pennsylvania, Philadelphia, Pennsylvania 19104-6323, United States;* orcid.org/0000-0002-6861-6421

Complete contact information is available at:
https://pubs.acs.org/10.1021/acscatal.2c06427

Author Contributions

S.B. performed all the calculations. S.B. and A.K. designed and executed the study with guidance from A.M.R. R.B.W. helped in understanding the surface reconstructions. All the authors wrote the manuscript together.

Notes

The authors declare no competing financial interest.

■ ACKNOWLEDGMENTS

The work was supported by the Department of Energy, Office of Science, Office of Basic Energy Sciences, under grant number DE-SC0019281. S.B. acknowledges the Vagelos Institute for Energy Science and Technology for the graduate fellowship. Computational support was provided by the National Energy Research Scientific Computing Center (NERSC), a U.S. Department of Energy, Office of Science User Facility located at Lawrence Berkeley National Laboratory, operated under Contract No. DE-AC02-05CH11231.

■ REFERENCES

(1) Abe, J.; Popoola, A.; Ajenifuja, E.; Popoola, O. Hydrogen energy, economy and storage: Review and recommendation. *Int. J. Hydrogen Energy* **2019**, *44*, 15072−15086.

(2) Lewis, N. S.; Nocera, D. G. Powering the planet: Chemical challenges in solar energy utilization. *Proc. Natl. Acad. Sci. U. S. A.* **2006**, *103*, 15729−15735.

(3) Popczun, E. J.; McKone, J. R.; Read, C. G.; Biacchi, A. J.; Wiltrout, A. M.; Lewis, N. S.; Schaak, R. E. Nanostructured Nickel Phosphide as an Electrocatalyst for the Hydrogen Evolution Reaction. *J. Am. Chem. Soc.* **2013**, *135*, 9267−9270.

(4) Lamoureux, P. S.; Singh, A. R.; Chan, K. pH Effects on Hydrogen Evolution and Oxidation over Pt(111): Insights from First-Principles. *ACS Catal.* **2019**, *9*, 6194−6201.

(5) Hansen, J. N.; Prats, H.; Toudahl, K. K.; Secher, N. M.; Chan, K.; Kibsgaard, J.; Chorkendorff, I. Is There Anything Better than Pt for HER? *ACS Energy Lett.* **2021**, *6*, 1175−1180.

(6) Lindgren, P.; Kastlunger, G.; Peterson, A. A. A challenge to the G ∼ 0 interpretation of hydrogen evolution. *ACS Catal.* **2020**, *10*, 121−128.

(7) Kibsgaard, J.; Tsai, C.; Chan, K.; Benck, J. D.; Nørskov, J. K.; Abild-Pedersen, F.; Jaramillo, T. F. Designing an improved transition metal phosphide catalyst for hydrogen evolution using experimental and theoretical trends. *Energy Environ. Sci.* **2015**, *8*, 3022−3029.

(8) Wang, H.; Tsai, C.; Kong, D.; Chan, K.; Abild-Pedersen, F.; Nørskov, J. K.; Cui, Y. Transition-metal doped edge sites in vertically aligned MoS_2 catalysts for enhanced hydrogen evolution. *Nano Research* **2015**, *8*, 566−575.

(9) Tsai, C.; Chan, K.; Nørskov, J. K.; Abild-Pedersen, F. Theoretical insights into the hydrogen evolution activity of layered transition metal dichalcogenides. *Surf. Sci.* **2015**, *640*, 133−140.

(10) Anantharaj, S.; Reddy, P. N.; Kundu, S. Core-oxidized amorphous cobalt phosphide nanostructures: an advanced and highly efficient oxygen evolution catalyst. *Inorg. Chem.* **2017**, *56*, 1742−1756.

(11) Kibsgaard, J.; Jaramillo, T. F.; Besenbacher, F. Building an appropriate active-site motif into a hydrogen-evolution catalyst with thiomolybdate $[Mo_3S_{13}]^{-2}$ clusters. *Nature Chem.* **2014**, *6*, 248−253.

(12) Kibsgaard, J.; Chen, Z.; Reinecke, B. N.; Jaramillo, T. F. Engineering the surface structure of MoS_2 to preferentially expose active edge sites for electrocatalysis. *Nat. Mater.* **2012**, *11*, 963−969.

(13) Laursen, A. B.; Wexler, R. B.; Whitaker, M. J.; Izett, E. J.; Calvinho, K. U. D.; Hwang, S.; Rucker, R.; Wang, H.; Li, J.; Garfunkel, E.; Greenblatt, M.; Rappe, A. M.; Dismukes, G. C. Climbing the Volcano of Electrocatalytic Activity while Avoiding Catalyst Corrosion: Ni_3P, a Hydrogen Evolution Electrocatalyst Stable in Both Acid and Alkali. *ACS Catal.* **2018**, *8*, 4408−4419.

(14) Laursen, A. B.; Patraju, K. R.; Whitaker, M. J.; Retuerto, M.; Sarkar, T.; Yao, N.; Ramanujachary, K. V.; Greenblatt, M.; Dismukes, G. C. Nanocrystalline Ni_5P_4: a hydrogen evolution electrocatalyst of exceptional efficiency in both alkaline and acidic media. *Energy Environ. Sci.* **2015**, *8*, 1027−1034.

(15) Pan, Y.; Liu, Y.; Zhao, J.; Yang, K.; Liang, J.; Liu, D.; Hu, W.; Liu, D.; Liu, Y.; Liu, C. Monodispersed nickel phosphide nanocrystals with different phases: synthesis, characterization and electrocatalytic properties for hydrogen evolution. *J. Mater. Chem. A* **2015**, *3*, 1656−1665.

(16) Kucernak, A. R.; Sundaram, V. N. N. Nickel phosphide: the effect of phosphorus content on hydrogen evolution activity and corrosion resistance in acidic medium. *J. Mater. Chem. A* **2014**, *2*, 17435−17445.

(17) Burchardt, T.; Hansen, V.; Våland, T. Microstructure and catalytic activity towards the hydrogen evolution reaction of electrodeposited NiP_x alloys. *Electrochimica acta* **2001**, *46*, 2761−2766.

(18) Huang, Z.; Chen, Z.; Chen, Z.; Lv, C.; Meng, H.; Zhang, C. $Ni_{12}P_5$ Nanoparticles as an Efficient Catalyst for Hydrogen Generation via Electrolysis and Photoelectrolysis. *ACS Nano* **2014**, *8*, 8121−8129.

(19) Feng, L.; Vrubel, H.; Bensimon, M.; Hu, X. Easily-prepared dinickel phosphide Ni_2P nanoparticles as an efficient and robust electrocatalyst for hydrogen evolution. *Phys. Chem. Chem. Phys.* **2014**, *16*, 5917−5921.

(20) Cao, S.; Chen, Y.; Wang, C.-J.; He, P.; Fu, W.-F. Highly efficient photocatalytic hydrogen evolution by nickel phosphide nanoparticles from aqueous solution. *Chem. Commun.* **2014**, *50*, 10427−10429.

(21) Liu, P.; Rodriguez, J. A. Catalysts for Hydrogen Evolution from the [NiFe] Hydrogenase to the $Ni_2P(001)$ Surface: The Importance of Ensemble Effect. *J. Am. Chem. Soc.* **2005**, *127*, 14871−14878.

(22) Reuter, K.; Scheffler, M. Composition and structure of the $RuO_2(110)$ surface in an O_2 and CO environment: Implications for the catalytic formation of CO_2. *Phys. Rev. B* **2003**, *68*, 045407.

(23) Cook, S.; Marks, L. D. Ab Initio Predictions of Double-Layer TiO_2-Terminated $SrTiO_3(001)$ Surface Reconstructions. *J. Phys. Chem. C* **2018**, *122*, 21991−21997.

(24) Di Valentin, C.; Pacchioni, G.; Selloni, A. Electronic Structure of Defect States in Hydroxylated and Reduced Rutile $TiO_2(110)$ Surfaces. *Phys. Rev. Lett.* **2006**, *97*, 166803.

(25) Martirez, J. M. P.; Morales, E. H.; Saidi, W. A.; Bonnell, D. A.; Rappe, A. M. Atomic and Electronic Structure of the $BaTiO_3(001)$ $\sqrt{5} \times \sqrt{5}R26.6°$ Surface Reconstruction. *Phys. Rev. Lett.* **2012**, *109*, 256802.

(26) Rogal, J.; Reuter, K.; Scheffler, M. Thermodynamic stability of PdO surfaces. *Phys. Rev. B* **2004**, *69*, 075421.

(27) Wexler, R. B.; Qiu, T.; Rappe, A. M. Automatic Prediction of Surface Phase Diagrams Using Ab Initio Grand Canonical Monte Carlo. *J. Phys. Chem. C* **2019**, *123*, 2321−2328.

(28) Li, W.-X.; Stampfl, C.; Scheffler, M. Subsurface oxygen and surface oxide formation at Ag(111): A density-functional theory investigation. *Phys. Rev. B* **2003**, *67*, 045408.

(29) Abroshan, H.; Bothra, P.; Back, S.; Kulkarni, A.; Nørskov, J. K.; Siahrostami, S. Ultrathin Cobalt Oxide Overlayer Promotes Catalytic Activity of Cobalt Nitride for the Oxygen Reduction Reaction. *J. Phys. Chem. C* **2018**, *122*, 4783−4791.

(30) Wexler, R. B.; Martirez, J. M. P.; Rappe, A. M. Active Role of Phosphorus in the Hydrogen Evolving Activity of Nickel Phosphide (0001) Surfaces. *ACS Catal.* **2017**, *7*, 7718−7725.

(31) Garrity, K.; Kakekhani, A.; Kolpak, A.; Ismail-Beigi, S. Ferroelectric surface chemistry: First-principles study of the $PbTiO_3$ surface. *Phys. Rev. B* **2013**, *88*, 045401.
(32) Rasmussen, M. K.; Foster, A. S.; Hinnemann, B.; Canova, F. F.; Helveg, S.; Meinander, K.; Martin, N. M.; Knudsen, J.; Vlad, A.; Lundgren, E.; Stierle, A.; Besenbacher, F.; Lauritsen, J. V. Stable Cation Inversion at the $MgAl_2O_4$(100) Surface. *Phys. Rev. Lett.* **2011**, *107*, 036102.
(33) Martirez, J. M. P.; Kim, S.; Morales, E. H.; Diroll, B. T.; Cargnello, M.; Gordon, T. R.; Murray, C. B.; Bonnell, D. A.; Rappe, A. M. Synergistic Oxygen Evolving Activity of a TiO_2-Rich Reconstructed $SrTiO_3$(001) Surface. *J. Am. Chem. Soc.* **2015**, *137*, 2939−2947.
(34) Polo-Garzon, F.; Fung, V.; Liu, X.; Hood, Z. D.; Bickel, E. E.; Bai, L.; Tian, H.; Foo, G. S.; Chi, M.; Jiang, D.-e.; Wu, Z. Understanding the Impact of Surface Reconstruction of Perovskite Catalysts on CH_4 Activation and Combustion. *ACS Catal.* **2018**, *8*, 10306−10315.
(35) Li, Y.-F.; Aschauer, U.; Chen, J.; Selloni, A. Adsorption and Reactions of O_2 on Anatase TiO_2. *Acc. Chem. Res.* **2014**, *47*, 3361−3368.
(36) Chakraborty, D.; Smitshuysen, T. E. L.; Kakekhani, A.; Jespersen, S. P. F.; Banerjee, S.; Krabbe, A.; Hagen, N.; Silva, H.; Just, J.; Damsgaard, C. D.; et al. Reversible Atomization and Nano-Clustering of Pt as a Strategy for Designing Ultra-Low-Metal-Loading Catalysts. *J. Phys. Chem. C* **2022**, *126*, 16194−16203.
(37) Kondori, A.; Jiang, Z.; Esmaeilirad, M.; Tamadoni Saray, M.; Kakekhani, A.; Kucuk, K.; Navarro Munoz Delgado, P.; Maghsoudipour, S.; Hayes, J.; Johnson, C. S.; et al. Kinetically stable oxide overlayers on Mo_3P nanoparticles enabling lithium-air batteries with low overpotentials and long cycle life. *Adv. Mater.* **2020**, *32*, 2004028.
(38) Qiu, T.; Tu, B.; Saldana-Greco, D.; Rappe, A. M. Ab Initio Simulation Explains the Enhancement of Catalytic Oxygen Evolution on $CaMnO_3$. *ACS Catal.* **2018**, *8*, 2218−2224.
(39) Banerjee, S.; Kakekhani, A.; Wexler, R. B.; Rappe, A. M. Mechanistic Insights into CO_2 Electroreduction on Ni_2P: Understanding Its Selectivity toward Multicarbon Products. *ACS Catal.* **2021**, *11*, 11706−11715.
(40) Calvinho, K. U. D. Transition Metal Phosphides for High Energy Efficiency Electrocatalytic CO_2 Reduction: Investigating Mechanisms and Structure-Activity Relationship. Ph.D. Thesis, Rutgers, The State University of New Jersey, School of Graduate Studies, 2020.
(41) Popczun, E. J.; Read, C. G.; Roske, C. W.; Lewis, N. S.; Schaak, R. E. Highly Active Electrocatalysis of the Hydrogen Evolution Reaction by Cobalt Phosphide Nanoparticles. *Angew. Chem., Int. Ed.* **2014**, *53*, 5427−5430.
(42) Callejas, J. F.; McEnaney, J. M.; Read, C. G.; Crompton, J. C.; Biacchi, A. J.; Popczun, E. J.; Gordon, T. R.; Lewis, N. S.; Schaak, R. E. Electrocatalytic and Photocatalytic Hydrogen Production from Acidic and Neutral-pH Aqueous Solutions Using Iron Phosphide Nanoparticles. *ACS Nano* **2014**, *8*, 11101−11107.
(43) McEnaney, J. M.; Crompton, J. C.; Callejas, J. F.; Popczun, E. J.; Biacchi, A. J.; Lewis, N. S.; Schaak, R. E. Amorphous Molybdenum Phosphide Nanoparticles for Electrocatalytic Hydrogen Evolution. *Chem. Mater.* **2014**, *26*, 4826−4831.
(44) Wexler, R. B.; Martirez, J. M. P.; Rappe, A. M. Chemical Pressure-Driven Enhancement of the Hydrogen Evolving Activity of Ni_2P from Nonmetal Surface Doping Interpreted via Machine Learning. *J. Am. Chem. Soc.* **2018**, *140*, 4678−4683.
(45) Lim, H.-K.; Shin, H.; Goddard, W. A.; Hwang, Y. J.; Min, B. K.; Kim, H. Embedding Covalency into Metal Catalysts for Efficient Electrochemical Conversion of CO_2. *J. Am. Chem. Soc.* **2014**, *136*, 11355−11361.
(46) Ghosh, S.; Kadam, S. R.; Kolatkar, S.; Neyman, A.; Singh, C.; Enyashin, A. N.; Bar-Ziv, R.; Bar-Sadan, M. W doping in $Ni_{12}P_5$ as a platform to enhance overall electrochemical water splitting. *ACS Appl. Mater. Interfaces* **2022**, *14*, 581−589.
(47) Jiang, P.; Liu, Q.; Sun, X. NiP_2 nanosheet arrays supported on carbon cloth: an efficient 3D hydrogen evolution cathode in both acidic and alkaline solutions. *Nanoscale* **2014**, *6*, 13440−13445.
(48) Owens-Baird, B.; Xu, J.; Petrovykh, D. Y.; Bondarchuk, O.; Ziouani, Y.; González-Ballesteros, N.; Yox, P.; Sapountzi, F. M.; Niemantsverdriet, H.; Kolen'ko, Y. V.; Kovnir, K. NiP_2: A story of two divergent polymorphic multifunctional materials. *Chem. Mater.* **2019**, *31*, 3407−3418.
(49) Xin, H.; Vojvodic, A.; Voss, J.; Nørskov, J. K.; Abild-Pedersen, F. Effects of d-band shape on the surface reactivity of transition-metal alloys. *Phys. Rev. B* **2014**, *89*, 115114.
(50) Medford, A. J.; Vojvodic, A.; Hummelshøj, J. S.; Voss, J.; Abild-Pedersen, F.; Studt, F.; Bligaard, T.; Nilsson, A.; Nørskov, J. K. From the Sabatier principle to a predictive theory of transition-metal heterogeneous catalysis. *J. Catal.* **2015**, *328*, 36−42.
(51) Hammer, B.; Morikawa, Y.; Nørskov, J. K. Chemisorption at Metal Surfaces and Overlayers. *Phys. Rev. Lett.* **1996**, *76*, 2141−2144.
(52) Nørskov, J. K.; Abild-Pedersen, F.; Studt, F.; Bligaard, T. Density functional theory in surface chemistry and catalysis. Proceedings of the National Academy of Sciences. *Proc. Natl. Acad. Sci. U. S. A.* **2011**, *108*, 937−943.
(53) Wexler, R. B.; Martirez, J. M. P.; Rappe, A. M. Stable Phosphorus-Enriched (0001) Surfaces of Nickel Phosphides. *Chem. Mater.* **2016**, *28*, 5365−5372.
(54) Suzuki, S.; Moula, G. M.; Miyamoto, T.; Nakagawa, Y.; Kinosthita, K.; Asakura, K.; Oyama, S. T.; Otani, S. Scanning Tunneling Microscopy and Photoemission Electron Microscopy Studies on Single Crystal Ni_2P Surfaces. *J. Nanosci. Nanotechnol.* **2009**, *9*, 195−201.
(55) Hernandez, A. B.; Ariga, H.; Takakusagi, S.; Kinoshita, K.; Suzuki, S.; Otani, S.; Oyama, S. T.; Asakura, K. Dynamical LEED analysis of Ni_2P(0001)-1 × 1: Evidence for P-covered surface structure. *Chem. Phys. Lett.* **2011**, *513*, 48−52.
(56) Wang, H.; Xie, Y.; Cao, H.; Li, Y.; Li, L.; Xu, Z.; Wang, X.; Xiong, N.; Pan, K. Flower-Like Nickel Phosphide Microballs Assembled by Nanoplates with Exposed High-Energy (001) Facets: Efficient Electrocatalyst for the Hydrogen Evolution Reaction. *ChemSusChem* **2017**, *10*, 4899−4908.
(57) Nørskov, J. K.; Studt, F.; Abild-Pedersen, F.; Bligaard, T. *Fundamental concepts in heterogeneous catalysis*; John Wiley & Sons, 2014.
(58) Zheng, Y.; Jiao, Y.; Vasileff, A.; Qiao, S.-Z. The hydrogen evolution reaction in alkaline solution: from theory, single crystal models, to practical electrocatalysts. *Angew. Chem., Int. Ed.* **2018**, *57*, 7568−7579.
(59) McCrum, I. T.; Koper, M. T. The role of adsorbed hydroxide in hydrogen evolution reaction kinetics on modified platinum. *Nature Energy* **2020**, *5*, 891−899.
(60) Feng, L.; Vrubel, H.; Bensimon, M.; Hu, X. Easily-prepared dinickel phosphide (Ni_2P) nanoparticles as an efficient and robust electrocatalyst for hydrogen evolution. *Phys. Chem. Chem. Phys.* **2014**, *16*, 5917−5921.
(61) Zhang, Z.; Jiang, Y.; Zheng, X.; Sun, X.; Guo, Y. Electro-depositing ultra-thin $Ni(OH)_2$ amorphous film on Ni_2P nanosheets array: an efficient strategy toward greatly enhanced alkaline hydrogen evolution reaction. *New J. Chem.* **2018**, *42*, 11285−11288.
(62) Hansen, M. H.; Stern, L.-A.; Feng, L.; Rossmeisl, J.; Hu, X. Widely available active sites on Ni_2P for electrochemical hydrogen evolution-insights from first principles calculations. *Phys. Chem. Chem. Phys.* **2015**, *17*, 10823−10829.
(63) Wang, X.; Hu, Q.; Li, G.; Wei, S.; Yang, H.; He, C. Regulation of the adsorption sites of Ni_2P by Ru and S co-doping for ultra-efficient alkaline hydrogen evolution. *Journal of Materials Chemistry A* **2021**, *9*, 15648−15653.
(64) Zhang, N.-N.; Li, J.; Xiao, H. The Key Role of Competition between Orbital and Electrostatic Interactions in the Adsorption on Transition Metal Single-Atom Catalysts Anchored by N-doped Graphene. *ChemCatChem.* **2022**, *14*, e202200275.

(65) Giannozzi, P.; et al. QUANTUM ESPRESSO: a modular and open-source software project for quantum simulations of materials. *J. Phys.: Condens. Matter* **2009**, *21*, 395502.
(66) Perdew, J. P.; Burke, K.; Ernzerhof, M. Generalized Gradient Approximation Made Simple. *Phys. Rev. Lett.* **1996**, *77*, 3865−3868.
(67) Nie, X.; Esopi, M. R.; Janik, M. J.; Asthagiri, A. Selectivity of CO_2 Reduction on Copper Electrodes: The Role of the Kinetics of Elementary Steps. *Angew. Chem., Int. Ed.* **2013**, *52*, 2459−2462.
(68) Cheng, T.; Xiao, H.; Goddard, W. A. Reaction Mechanisms for the Electrochemical Reduction of CO_2 to CO and Formate on the Cu(100) Surface at 298 K from Quantum Mechanics Free Energy Calculations with Explicit Water. *J. Am. Chem. Soc.* **2016**, *138*, 13802−13805.
(69) Rappe, A. M.; Rabe, K. M.; Kaxiras, E.; Joannopoulos, J. D. Optimized pseudopotentials. *Phys. Rev. B* **1990**, *41*, 1227−1230.
(70) Ramer, N. J.; Rappe, A. M. Designed nonlocal pseudopotentials for enhanced transferability. *Phys. Rev. B* **1999**, *59*, 12471−12478.
(71) *Opium: Pseudopotential generation project*. http://opium.sourceforge.net/ (accessed 2007-08-16).
(72) Grimme, S.; Antony, J.; Ehrlich, S.; Krieg, H. A consistent and accurate ab initio parametrization of density functional dispersion correction (DFT-D) for the 94 elements H-Pu. *J. Chem. Phys.* **2010**, *132*, 154104.
(73) Moellmann, J.; Grimme, S. DFT-D3 Study of Some Molecular Crystals. *J. Phys. Chem. C* **2014**, *118*, 7615−7621.
(74) Hujo, W.; Grimme, S. Comparison of the performance of dispersion-corrected density functional theory for weak hydrogen bonds. *Phys. Chem. Chem. Phys.* **2011**, *13*, 13942−13950.
(75) Ramalho, J. P. P.; Gomes, J. R. B.; Illas, F. Accounting for van der Waals interactions between adsorbates and surfaces in density functional theory based calculations: selected examples. *RSC Adv.* **2013**, *3*, 13085−13100.
(76) Davis, J. B. A.; Baletto, F.; Johnston, R. L. The Effect of Dispersion Correction on the Adsorption of CO on Metallic Nanoparticles. *J. Phys. Chem. A* **2015**, *119*, 9703−9709.
(77) Peterson, A. A.; Abild-Pedersen, F.; Studt, F.; Rossmeisl, J.; Nørskov, J. K. How copper catalyzes the electroreduction of carbon dioxide into hydrocarbon fuels. *Energy Environ. Sci.* **2010**, *3*, 1311−1315.
(78) Nørskov, J. K.; Rossmeisl, J.; Logadottir, A.; Lindqvist, L.; Kitchin, J. R.; Bligaard, T.; Jónsson, H. Origin of the Overpotential for Oxygen Reduction at a Fuel-Cell Cathode. *J. Phys. Chem. B* **2004**, *108*, 17886−17892.
(79) Rong, X.; Kolpak, A. M. Ab Initio Approach for Prediction of Oxide Surface Structure, Stoichiometry, and Electrocatalytic Activity in Aqueous Solution. The. *J. Phys. Chem. Lett.* **2015**, *6*, 1785−1789.

https://doi.org/10.1021/acscatal.2c06427
ACS Catal. 2023, 13, 4611−4621